Boundary-Layer Meteorol (2011) 139:457–485
DOI 10.1007/s10546-011-9590-8

ARTICLE

Estimation of Roughness Parameters Within Sparse Urban-Like Obstacle Arrays

Byung-Gu Kim · Changhoon Lee · Seokjun Joo · Ki-Cheol Ryu · Seogcheol Kim · Donghyun You · Woo-Sup Shim

Received: 2 September 2009 / Accepted: 19 January 2011 / Published online: 23 February 2011

Abstract We conduct wind-tunnel experiments on three different uniform roughness arrays composed of sparsely distributed rectangular cylinders for the estimation of surface parameters. Roughness parameters such as the roughness length z_0 and zero-plane displacement d are extracted using a best-fit approximation of the measured wind velocity. We also perform a large-eddy simulation (LES) to confirm that four sampling points are sufficient to surrogate a space average above the canopy layer of the sparse roughness arrays. We propose a new morphological model from a systematic analysis of experimental data on the arrays. The friction velocity predicted by the proposed model agrees well with the peak value of the measured Reynolds shear stress $(-\langle\overline{u'w'}\rangle)^{0.5}$. The proposed model is further validated in an additional wind-tunnel experiment conducted on a scaled configuration of a real urban area exposed to four wind directions. The proposed model is found to perform very well

B.-G. Kim · C. Lee (✉) · D. You
Department of Computational Science and Engineering, Yonsei University, Seoul 120-749, Korea
e-mail: clee@yonsei.ac.kr

Present Address:
B.-G. Kim
LG Electronics, Seoul, Korea

C. Lee
Department of Mechanical Engineering, Yonsei University, Seoul 120-749, Korea

S. Joo · K.-C. Ryu
TESolution, Anseong, Kyungi-do 456-825, Korea

S. Kim
Boolt Simulation, Seoul 137-840, Korea

D. You
Department of Mechanical Engineering, Carnegie Mellon University, Pittsburgh, PA 15213, USA

W.-S. Shim
Agency for Defense Development, Daejeon 305-600, Korea

particularly in the estimation of the friction velocity, readily leading to a better estimation of turbulence, which is essential for an accurate prediction of pollutant dispersion.

Keywords Morphological method · Roughness parameters · Surface parameters · Urban dispersion

1 Introduction

The dispersion of toxic material and chemical and biological agents that could be released by either accidental or nonaccidental events is an important issue today, especially for urban areas in which a large population resides. However, characteristics of boundary-layer flow in an urban area are substantially different from that in a rural area because of the presence of bluff obstacles on the ground such as buildings or other artificial structures (Jiménez 2004). An accurate characterization of a flow field in an urban area would lead to accurate prediction of dispersion. For example, the wind-speed profile in neutral conditions above an urban canopy and within the inertial sublayer is given by

$$\frac{u(z)}{u_*} = \frac{1}{\kappa}\ln\left(\frac{z-d}{z_0}\right), \tag{1}$$

where u_*, d, and z_0 are the friction velocity, zero-plane displacement, and aerodynamic roughness length, respectively. Here, κ (taken in this article to be 0.41) is the von Kármán constant. Parametrizations of a mean wind-speed profile within vegetative and urban canopies have been investigated previously. Cionco (1965) proposed the exponential profile using mixing length theory within a vegetative canopy, and Bentham and Britter (2003) suggested a constant velocity profile in a moderately densely packed array for more simplicity. Macdonald (2000) suggested a matching profile that consists of an exponential distribution below the canopy height and a modified logarithmic distribution above. Turbulence levels that directly influence dispersion are in most cases estimated by the friction velocity. These suggest that roughness parameters such as u_*, z_0, and d are essential variables in the characterization of the flow in urban areas. Therefore, it is crucial to estimate those parameters accurately for better prediction of urban dispersion. Both z_0 and d, however, are not directly measurable lengths, and thus these lengths and u_* need to be estimated by an indirect method. The best-fit method provides the roughness parameters with a decent precision; however, it requires observations moreover at several vertical levels, which is practically unattainable at the usual meteorological stations.

The land-use land-cover (LULC) method is based on a tabulated value of z_0 versus land-use type Stull (1988, pp. 378–381), and has been widely used in the application to dispersion models, such as SCIPUFF, AERMOD, and CALPUFF models. A problem with this method is that land-use categories are broadly defined and thus ambiguous. In an urban area, for example, building shapes and space or packing density are not properly accounted for in the LULC method.

A more elaborate estimation of z_0 and d is possible by considering the morphology, i.e., dimensions and arrangement of buildings, in an urban area. A morphological method typically depends on geometric parameters: the total plan building area (A_p), the total frontal building area (A_f) viewed from the wind direction, and the lot area (A_T) (see Fig. 1 for detailed definitions). Then, nondimensional parameters, which have been used in most morphological models (Lettau 1969; Counihan 1971; Theurer 1993; Petersen 1997; Grimmond and Oke 1999; Hanna and Britter 2002), are defined as $\lambda_f = A_f/A_T$ and $\lambda_p = A_p/A_T$. Macdonald

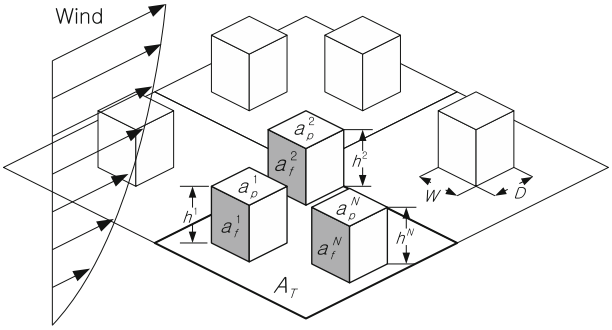

Fig. 1 Definitions of morphological parameters a_p^i, a_f^i, and h^i contributed by an ith obstacle in the lot area A_T. Total areas become $A_f = \sum_{i=1}^{N} a_f^i$, $A_p = \sum_{i=1}^{N} a_p^i$

et al. (1998) described a theoretical derivation of roughness lengths using a morphological model.

With increasing computing power, the use of computational fluid dynamics (CFD) is growing in the discipline of air quality and wind engineering (Hanna et al. 2006; Tamura 2008). Application of CFD is, however, acceptable for relatively small scales from the neighbourhood scale to the street scale, as defined by Britter and Hanna (2003). Thus the dispersion model relying on the parametrization is still required for the long time and long range dispersion prediction and for urgent measures against dispersion of a toxic agent.

In this study, we perform two types of wind-tunnel experiments: (i) flow over uniformly distributed sparse obstacle arrays; (ii) flow over a scale model of a real urban area. Using the datasets obtained from the uniform array experiments, a wind-profile method is utilized to estimate values of z_0 and d. Then an assessment of several morphological models is carried out. New relations for z_0 and d are proposed to compensate for errors in the z_0 estimation. The proposed model is found to better predict the friction velocity. This new model, when applied to a scaled urban area, is found to perform best among the models compared.

Section 2 provides a detailed explanation of wind-tunnel experiments and measured results. In Sect. 3, we perform a large-eddy simulation (LES) for the comparison of four-point and space averages. In Sect. 4, several models including Theurer (1993), Macdonald et al. (1998), Grimmond and Oke (1999), and Hanna and Britter (2002) are assessed, and a new model is proposed and validated. Section 5 concludes our study.

2 Wind-Tunnel Experiments

2.1 Wind Tunnel and Instrumentation

Wind field measurements were conducted in an open-circuit-type boundary-layer wind-tunnel that has a test section of 23.2 m × 8 m × 2.5 m (length × span × height) at the TESolution located in Anseong City in Korea. Two stages of wind tunnel experiments were performed to obtain information on the flow for the extraction of roughness parameters. The first stage consists of wind-tunnel tests on three idealized urban type roughness arrays such as the ones shown in the photograph of Fig. 2a. The second stage is made up of a wind tunnel test on a scale model of an urban area, a part of Daejeon City in Korea as shown in Fig. 2b.

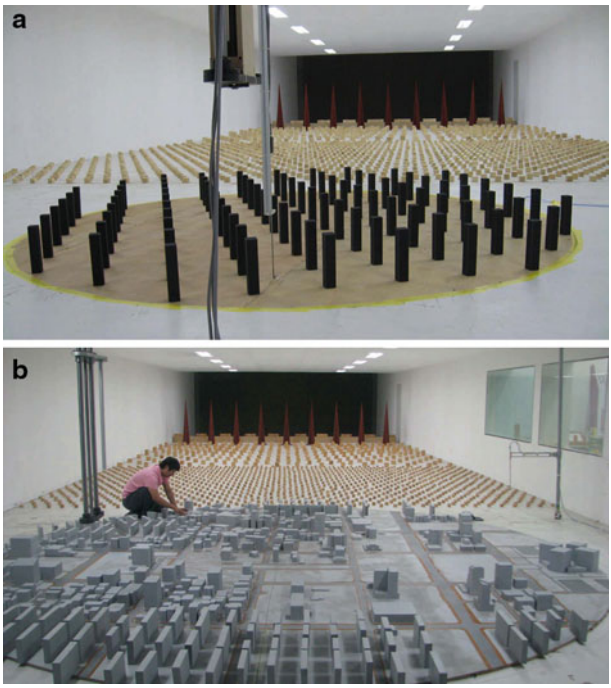

Fig. 2 Photographs of **a** experimental set-ups for the uniform roughness array A, and **b** the 1:300 scale model for a region of Daejeon City in Korea

Wind-tunnel experiments for the uniform arrays were designed to mimic flow over a terrain category exposure B. The Korean building code, the exposure B corresponds to a terrain with numerous closely spaced obstructions in the size of single-family dwellings or larger, or to a terrain with scattered obstructions with the medium height. The incoming mean wind profile for the exposure B was generated to yield a power-law profile,

$$\frac{u(z)}{u_r} = \left(\frac{z}{z_r}\right)^{\alpha}, \tag{2}$$

where u_r is the mean wind speed at the reference height z_r, and α is the power-law exponent for an exposure class. In the experiments, $u_r = 6\,\mathrm{m\,s^{-1}}$ and $z_r = 0.3\,\mathrm{m}$. For the exposure B, the exponent α is 0.22.

The flow velocity was measured using an x-probe hot-film anemometer (DANTEC 55R91 3-D Probe) for 20.48 sec at sampling frequency of 200 Hz at each measurement location. In the wind-tunnel experiment, the roughness Reynolds number, $Re_* \equiv u_* z_0/\nu$, should be high enough (>2) to satisfy Reynolds number independence (Schlichting and Gersten 2000), where ν is the kinematic viscosity of air. A study of Snyder and Castro (2002) showed that a rough wall can be regarded as aerodynamically rough if $Re_* > 1$, while Re_* as small as 0.5 was found to be sufficient over a rough wall composed of sharp-edged obstacles. This criterion is satisfied in the present experiments since the smallest Re_* is greater than 40.

The fetch before the measurement locations is about 1.28 m in the uniform arrays. In terms of z_0, it ranges between 80 and $750 z_0$, where z_0 is the value estimated by a best-fit method which will be explained later. Cheng and Castro (2002a) showed that $160 z_0$ is required for

Table 1 Morphological roughness parameters of arrays A, B, and C

Array	Parameters	Wind direction (°)									
		0	10	20	30	40	50	60	70	80	90
A ($\lambda_p = 0.02$, $H = 200$)	λ_f	0.10	0.12	0.13	0.14	0.14	0.14	0.14	0.13	0.12	0.1
	z_0	5.8	1.7	2.0	2.2	3.1	3.2	1.9	2.4	3.2	7.0
	d	91.	160.	157.	153.	145.	147.	164.	151.	128.	72.
B ($\lambda_p = 0.06$, $H = 200$)	λ_f	0.10	0.15	0.2	0.24	0.28	0.30	0.32	0.32	0.32	0.31
	z_0	5.3	4.8	2.7	5.3	5.7	9.7	11.	12.	16.	14.
	d	117.	136.	161.	153.	162.	155.	154.	153.	146.	147.
C ($\lambda_p = 0.12$, $H = 240$)	λ_f	0.12	0.18	0.24	0.28	0.32	0.35	0.37	0.38	0.38	0.36
	z_0	2.4	1.4	3.0	3.4	3.3	3.3	2.8	3.2	3.4	4.0
	d	173.	198.	189.	202.	231.	233.	233.	233.	222.	211.

Here z_0 and d are the values that were obtained from the best-fit method. The length unit is mm

the development of an equilibrium boundary layer. In most cases, however, a shorter distance was sufficient for a fully developed mean wind speed and turbulence statistics. An equilibrium is typically found after three to four rows of obstacles (Macdonald et al. 2000; Hanna et al. 2002). Therefore, the present experimental configurations satisfy the above criteria.

It is possible to provide various values of λ_f by rotating a roughness array on a turntable, thereby changing the wind direction, θ, relative to the array. For uniform roughness arrays, the turntable is rotated by 10° until achieving 90° in the counterclockwise direction, and this allows us to conduct ten experiments for each uniform array. For the non-uniform scale model, experiments for four wind directions, 180, 225, 270, and 315° were conducted.

2.2 Uniform Roughness Arrays

Uniform roughness arrays consist of regularly arranged square or rectangular column blocks on a disk with a diameter of 3 m, and represent idealized buildings of 1:250 scale for the wind exposure B. The types of roughness arrays are selected to imitate common modern cities in Korea. Figure 3 shows configurations of uniform array A, B, and C, and dimensions of three different blocks forming the arrays. All blocks have surfaces that are covered with sandpapers of 100 grits to improve the local flow similarity, although the roughness Reynolds numbers are sufficiently high. Table 1 shows ranges of morphological parameters of the three arrays obtained using a best-fit method, which will be explained in detail in Sect. 2.4.

The mean wind speed and turbulence intensities were measured at four different locations shown in Fig. 3 at 49 levels in the range of 2 mm–1,200 mm, which will be used to obtain spatially-averaged flow quantities.

2.3 Non-uniform Roughness Arrays

A 1:300 scale model of an urban area (latitude 36°21′, longitude 127°23′) of Daejeon City in Korea was replicated for a wind-tunnel experiment (Fig. 2b). The target area for a model

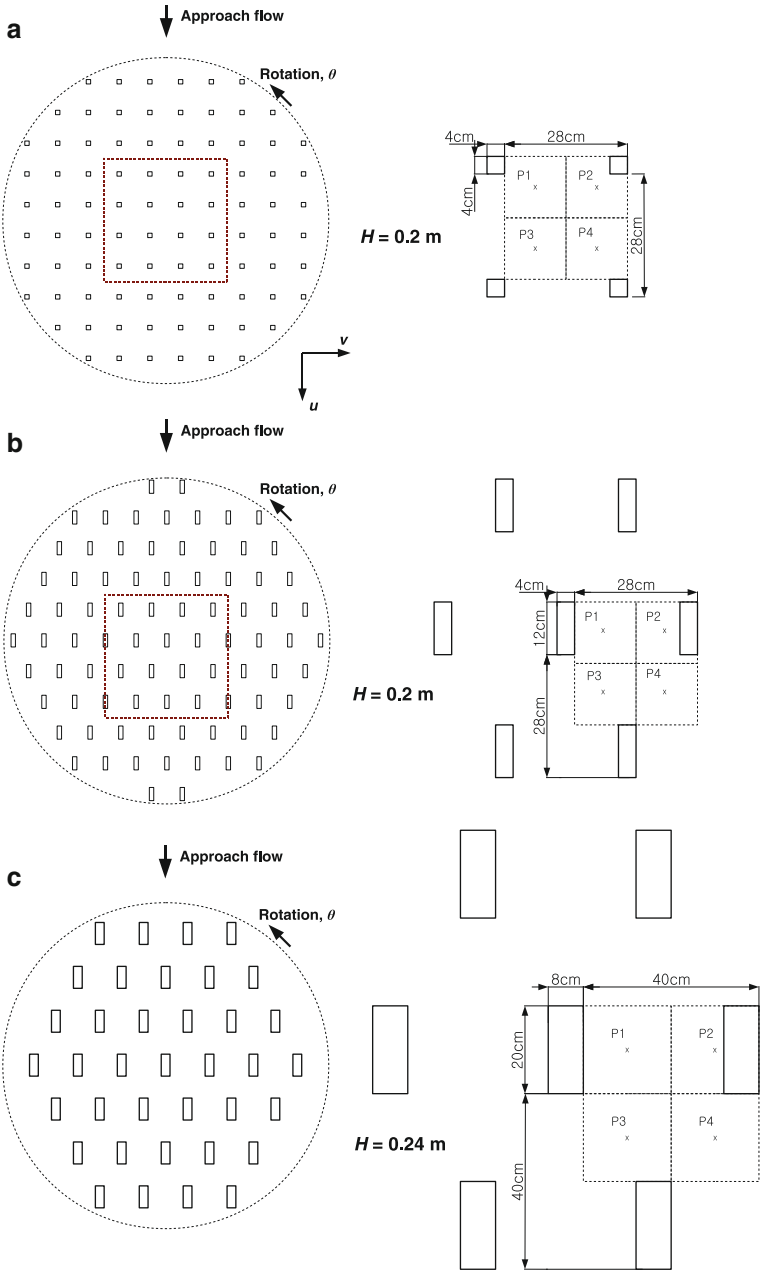

Fig. 3 Configurations and dimensions of the uniform arrays A, B, and C. *Red boxes* in array A and B represent computational domains. Four measurement locations adjacent to centre of arrays are marked by '×'

assessment is a flat terrain containing buildings of medium height as shown in Fig. 4. Building information for the model construction was obtained from a 1:10,000 scale map as CAD drawings, which was provided by the National Geographic Information Institute of Korea

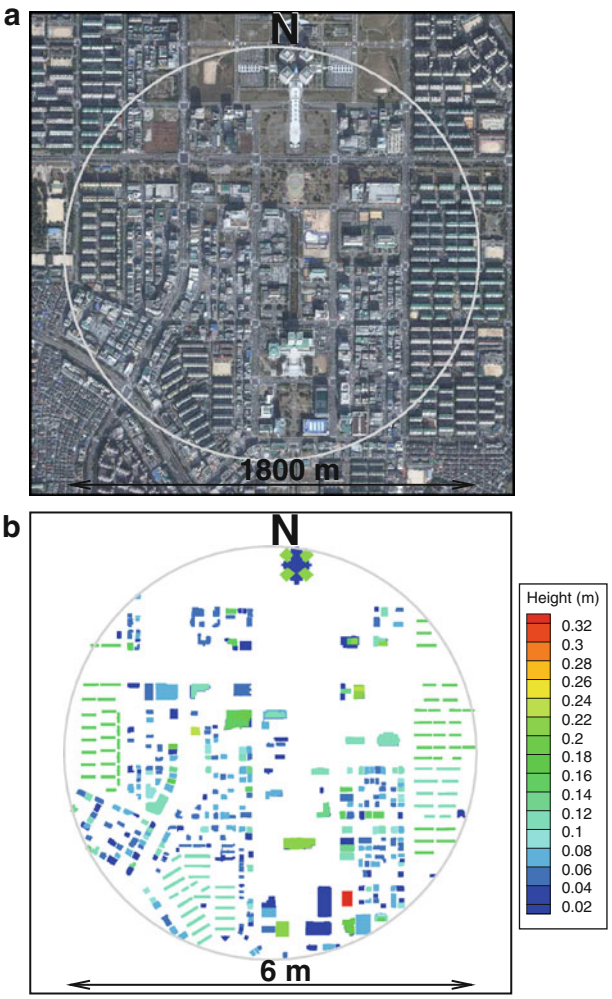

Fig. 4 **a** Aerial photo of the region of Daejeon City and **b** the height distribution in a replicated scale model for a wind-tunnel experiment

and an on-the-spot survey. Scaled building structures were made of acrylic or styrofoam in detail, while trees and minor irregularities of the surface were neglected.

Measurements were made at 40 locations, ten per each wind direction, shown in Fig. 5 and at 20 elevations within $10\,\text{mm} < z < 400\,\text{mm}$ for each location. Wind directions for the measurement include the northwest, the west, the southwest and the south, which were selected due to the frequent occurrence in this region.

2.4 Extraction of Roughness Parameters

For a fully developed wind field over a uniform array, the spatially-averaged wind speed should be obtained by averaging the wind speed over one periodic domain. For our uniform roughness array the spatially-averaged quantity was obtained by averaging the data at four

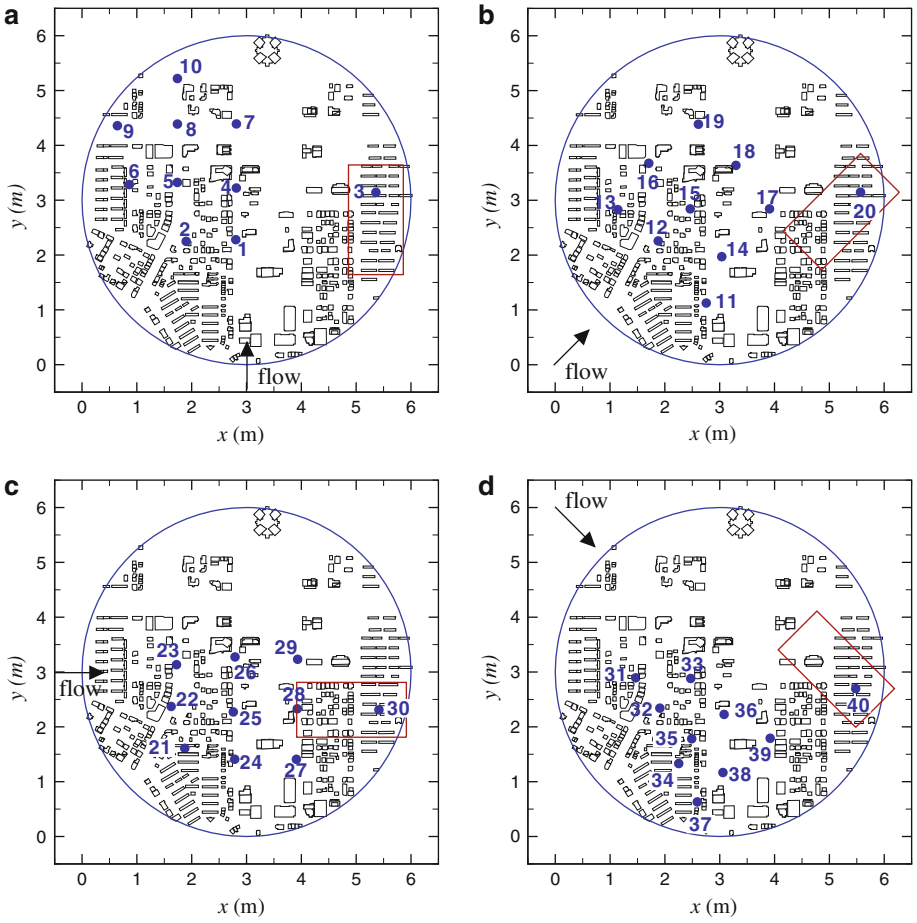

Fig. 5 Wind measurement locations (denoted by *numbers*) in the non-uniform roughness array (Daejeon, Korea) for wind directions **a** 180°, **b** 225°, **c** 270° and **d** 315°. *Rectangles* shown in **a**, **b**, **c**, and **d** represent the shape of the lot area corresponding to the measurement point aligned with the wind direction

locations in a periodic domain as marked by '×' in Fig. 3 due to measurement limitation. Cheng and Castro (2002b) showed that a four-point averaging is sufficient to obtain a spatially-averaged wind speed over the canopy height in the staggered or aligned arrays whose packing densities, λ_p, were 0.25. It has been known, from a direct numerical simulation (Coceal et al. 2007) and an observational study (Christen et al. 2009), that turbulent statistics, particularly the higher moments, are not spatially uniform below the canopy height. Coceal et al. (2007) showed that how many sampling points are required to achieve a sufficiently averaged quantity. Figure 12 in Coceal et al. (2007) shows that even three sampling locations are sufficient for averaging immediately below the canopy height. They concluded that a small number of sampling points located symmetrically are sufficient for a good representative spatially-averaged profile of the flow statistics including second-order moment even within the canopy. In our study only the data above the canopy height, which is believed to be less inhomogeneous than below, are used to assess the existing models. For the further verification of the assumption, we conducted an LES of a wind-tunnel experiment in Sect. 3.

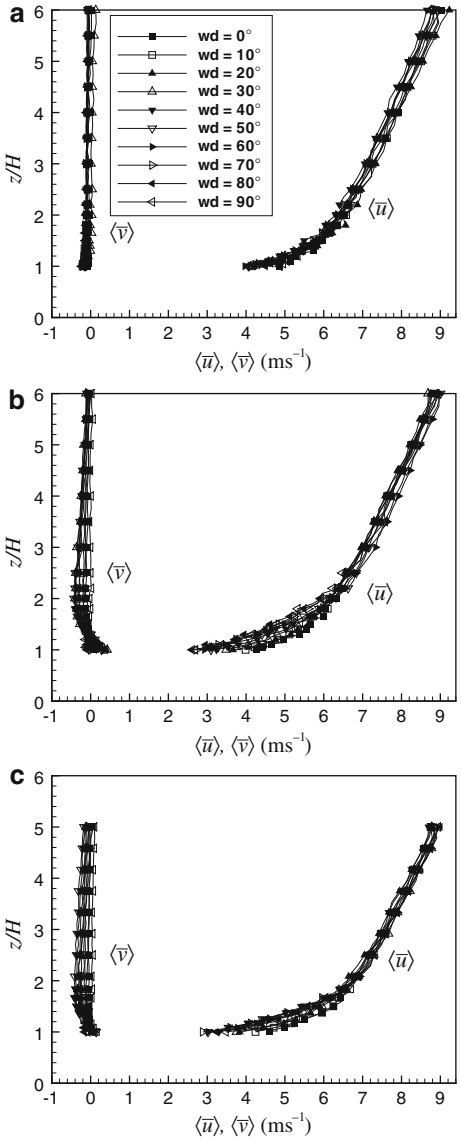

Fig. 6 Spatially averaged mean wind speed for each wind direction over the uniform arrays A, B, and C

Wind-speed profiles obtained by a four-point average are shown in Fig. 6 for each wind direction. Hereinafter, all profiles of the mean velocity and turbulence statistics for uniform arrays represent values that were obtained from four-point horizontal averaging denoted by $\langle\,\rangle$.

Cheng and Castro (2002b) measured u_* directly from the form drag arising due to the pressure difference between the front and back faces of a block. A practical and reliable way to estimate u_* is to use $u_*^2 = -\overline{u'w'}$ in the constant stress layer. In an urban type rough wall boundary layer, however, often the constant stress layer is not well established. Cheng and Castro (2002b) deduced u_* from a measured shear stress profile within the inertial sublayer

or within the roughness sublayer. They found that u_* deduced by averaging $-\overline{u'w'}$ in both layers is significantly lower than that obtained from a direct measurement of the form drag. Macdonald et al. (2002) proposed the averaged Reynolds stress in the layer between H and $2H$ as a good estimate of u_*^2. On the other hand, Rotach (2001) suggested that the peak value of the Reynolds stress, $MAX((-\overline{u'w'})^{0.5})$, be a good estimate of the friction velocity. A detailed study for the determination of u_* using a wind profile was extensively performed by Kastner-Klein and Rotach (2004).

In this study, friction velocities were obtained by three different methods: a best-fit method using a non-linear curve-fitting above the canopy layers; the maximum method that takes $MAX\left(\left(-\langle\overline{u'w'}\rangle\right)^{0.5}\right)$; and the average method averaging $\left(-\langle\overline{u'w'}\rangle\right)^{0.5}$ within H and $2H$, and are compared in Fig. 7. Using the best-fit method, u_*, z_0, and d were deduced simultaneously in this study. The best-fit was performed for every streamwise mean velocity profile shown in Fig. 6. It has been recommended to perform the best-fit in the inertial sublayer above the roughness sublayer. In boundary-layer flows over a vegetation canopy or urban areas with height variation, the upper bound of the roughness sublayer is known to be two to five times the mean height of the obstacles. It is vague, however, in the uniform height roughness array (Cheng and Castro 2002b). Theurer et al. (1992) found that the disturbances due to obstacles extend to a height differently in accordance with the patterns of roughness array. For a uniform pattern in their wind-tunnel experiments, it extends to about the canopy height itself, while that of the non-uniform height array extends to about twice height of the tallest building. It is worth noting that the vertical range for the best-fit is not uniquely defined (Petersen 1997; Cheng and Castro 2002b) but depends on the specific roughness array. Recently, it is reported that performing the best-fit within both the inertial sublayer and roughness sublayer results in a better prediction of u_* than the best-fit in the inertial sublayer only. Cheng and Castro (2002b) and Hagishima et al. (2009) performed best-fit in both layers for the estimation of the roughness parameters. The approach would be advocated when the logarithmic region can be extended to the roughness sublayer (Ploss et al. 2000).

Determination of the ranges of roughness sublayer and inertial sublayer was difficult using the profiles of wind speed and turbulent statistics in wind-tunnel experiments. In the sparse uniform roughness array, the influence of the obstacles on flow over the canopy layer may be weak. Thus we can take advantage of fitting a logarithmic profile to the experimental wind data above the canopy height. Ranges of $H < z < 5H$ for arrays A and B and $1.125H < z < 4.17H$ for array C resulted in good representative logarithmic profiles. Raupach et al. (1980) found that the effect of obstacle wake is important for $z < H + 1.5W$, where W is the obstacle width, which is insignificant for the uniform arrays in this study. Thus it reasonably validates the logarithmic curve-fit approach above the canopy layer equipped with tall and sparse roughness elements. Different fitting ranges such as $1.1H < z < 5H$ and $1.2H < z < 5H$, thus avoiding obstacle corner region, were also tested, resulting in no significant change in roughness parameters.

It was found that misalignment occurs between the approaching flow and the mean flow above the canopy layer for oblique wind direction cases. Figure 6 shows that the lateral component of wind has a non-zero value for oblique wind cases, which indicates that the wind vector forms a spiral line aloft rather than stays in a plane. Maximum values of $\langle\overline{v}\rangle$ are found at the canopy height while minimum values are found between 1.6–1.9 z/H for arrays B and C. It is hard to fit a spiralling wind profile to the logarithmic profile. Fortunately, lateral components are significantly smaller than streamwise components. Thus, only $\langle\overline{u}\rangle$ was used for the curve-fit instead of using the total wind vector, which implies that lateral stress $\langle\overline{v'w'}\rangle$ is neglected.

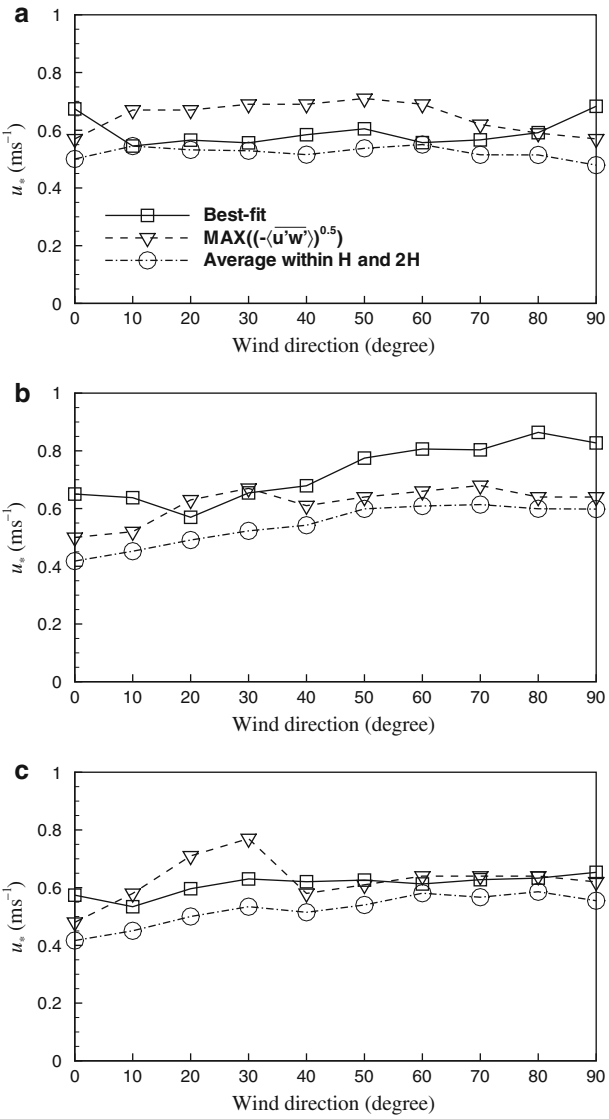

Fig. 7 Comparisons of u_* estimated using three different methods. **a** Array A; **b** array B; **c** array C

Before discussing the result obtained by the best-fit method, an uncertainty analysis for the best-fit is conducted here. The residuals for the logarithmic curve-fit are

$$e_i(u_*, z_0, d) = u_i - \frac{u_*}{\kappa} \ln\left(\frac{z_i - d}{z_0}\right), \tag{3}$$

where u_i is an experimental wind speed at a height z_i. Then the values of u_*, z_0, and d were iteratively estimated to minimize the error $\sum e_i^2$ using a subroutine DRNLIN for non-linear regression provided in the IMSL STAT/Library (Visual Numerics Inc. 1997). We checked the normalized error $E = \sum (e_i/u_i)^2/n$ for all datasets, where n is the number of measurement levels used for the non-linear regression. The range of the normalized error is

$8.4 \times 10^{-5} < E < 7.8 \times 10^{-4}$, which is small enough. It is known that the performance of a non-linear regression depends on the initial value. However, the differences in parameter values due to different initial conditions were found to be negligibly small such as 10^{-7}–10^{-6} when the parameters converge, suggesting that the parameters converge to unique values through a non-linear regression process. The fact that d in most cases converges to a reasonable value when compared with other models' prediction suggests a correct regression.

Friction velocities predicted by the averaging method are consistently smaller than the values predicted by other methods. This finding is consistent with that of Cheng and Castro (2002b). For the array A with a wind direction of 010–070°, friction velocities estimated by the maximum method are higher than those obtained using the best-fit because one (or more) hot-wire anemometers among four was positioned where turbulence is enhanced due to the wake immediately behind the blocks. It is worth noting that the estimation using the maximum value does not always predict a higher friction velocity than that provided by the best-fit (e.g., array B, 40–90°). For the array C with a wind direction 040–090°, predictions by the best-fit and the maximum methods collapse almost perfectly.

In real urban areas, securing a sufficient fetch for an equilibrium boundary layer often fails due to the heterogeneity of urban buildings. In this case, the upper portion of the profile higher than the roughness sublayer may carry the characteristics of the upstream flow that is not adjusted to the local surface (Cheng and Castro 2002a). Therefore, selecting u_* inevitably from the peak or average value of the shear stress mostly in the roughness sublayer is an alternative measure when a sufficient fetch is unobtainable or non-existent.

In summary, estimates by these three methods and comparisons against each other for three arrays in Fig. 7 confirm that a reasonable estimation of u_* can be made by any one of these methods. Therefore, assessment of models in the prediction of u_* will be carried out against u_* predicted by the best-fit method or $MAX((-\overline{u'w'})^{0.5})$.

3 Large-Eddy Simulation

3.1 Governing Equation and Numerical Setup

In this section, large-eddy simulations were conducted to numerically simulate the wind-tunnel experiment of the arrays A and B to check how well the four-point average used in the experiment approximates a space average. The space average was performed for the plane occupied by air (without solid volume). The LES code is based on the Fire Dynamics Simulator (McGrattan et al. 2009a) suitable for the simulation of flow around a complex geometry. Verification and validation of the code are provided in McDermott et al. (2009) and McGrattan et al. (2009b) in detail. The filtered Navier–Stokes equations in the Cartesian coordinate read,

$$\frac{\partial u_i}{\partial x_i} = 0, \tag{4}$$

$$\frac{\partial u_i}{\partial t} + \frac{\partial u_i u_j}{\partial x_j} = -\frac{1}{\rho}\left(\frac{\partial p}{\partial x_i} + \delta_{i1}\frac{\partial \langle p \rangle}{\partial x_1} + \delta_{i2}\frac{\partial \langle p \rangle}{\partial x_2}\right) + \frac{\partial}{\partial x_j}\left(-\tau_{ij} + \nu\frac{\partial u_i}{\partial x_j}\right), \tag{5}$$

where u_i, p, and τ_{ij} are the filtered velocity, pressure, and subgrid-scale stress tensor, respectively, ρ and ν are the density and kinematic viscosity of air, respectively and δ_{ij} is the Kronecker-delta. For the τ_{ij}, the Smagorinsky model was used with the Smagorinsky coefficient $C_s = 0.1$ as recommended by Shah (1998). The LES code adopts a second-order finite

difference approximation to Eqs. 4 and 5 on a rectangular-linear mesh. Time advancement is achieved using an explicit second-order Runge–Kutta scheme.

Computational domains containing 4×4 obstacles with a dimension of $1.12\,\mathrm{m} \times 1.12\,\mathrm{m} \times 2.4\,\mathrm{m}$ for the arrays A and B are illustrated in Fig. 3. Periodic boundary conditions were imposed for horizontal directions, and the logarithmic wall model of Werner and Wengle (1992) was applied on solid surfaces. Obstacles were symmetrically distributed on both bottom and top walls to maintain the free-stream condition at the channel centre height. Number of grid points on a rectilinear grid system were 280, 280, and 120 in x_1, x_2 (horizontal), and x_3 (wall-normal) directions, respectively. Uniform grids were employed in horizontal space and non-uniform in the vertical direction to cluster grid points in the vicinity of the canopy height.

In the numerical simulation, the turbulent flow along a certain wind direction θ was maintained by imposing a constant pressure gradient vector composed of $\partial \langle p \rangle / \partial x_1$ and $\partial \langle p \rangle / \partial x_2$. Numerical simulations were initiated with uniform horizontal velocity with weak random noises. For all cases, statistics were accumulated for 50 s after the turbulent flow reaches a statistically steady state.

3.2 Mean Flow Statistics

The mean pressure gradient was adjusted to match the mean wind speed measured in the experiment. The mean streamwise velocity obtained from the LES for array A with $\theta = 0, 40°$ and for array B with $\theta = 30, 60°$ are shown in Fig. 8. It is clear that in the region above the canopy layer, $z > H (= 0.2\,\mathrm{m})$, one-point velocity profiles at four locations are indistinguishable not only from each other but also from the four-point average. In the same range, the four-point average and the space average are very close to each other. Although there are some differences in velocity gradient among four different points near H, the four-point average and the space average are very close to each other. This indicates that four sampling points even for the velocity gradient are sufficient to provide a surrogate for the space average for our wind-tunnel experiments. It can provide a useful means when the velocity gradient is used for the parametrization of the turbulent momentum flux, i.e., the K-theory approach over urban-like obstacles (Santiago and Martilli 2010). Below the canopy layer the four-point average and one-point statistics are all different from the space average for arrays A and B. As indicated by Coceal et al. (2007), selecting sampling points in each of the distinct flow regimes is crucial to obtaining a good representative spatially-averaged profile.

As shown in Fig. 8, dispersive stresses (Raupach et al. 1986), $\langle \tilde{u}\tilde{w} \rangle$, where $\tilde{()} = \bar{()} - \langle \bar{()} \rangle$, above the canopy layer decrease rapidly and are very small compared with the velocity magnitude, confirm that the statistics were collected over sufficiently long time as noted by Coceal et al. (2006) and more importantly that the flow above the canopy height is nearly homogeneous. Note that in Fig. 8, $(\langle \tilde{u}\tilde{w} \rangle)^{0.5}$ is plotted instead of $\langle \tilde{u}\tilde{w} \rangle$ for the comparison with velocity.

4 Assessment of Morphological Models

Theurer (1993), Macdonald et al. (1998), Grimmond and Oke (1999), and Hanna and Britter (2002) suggested models to estimate both z_0 and d. Lettau (1969), Counihan (1971), and Petersen (1997) suggested models for only z_0. In our study, four existing morphological models, Hanna and Britter, rule-of-thumb suggested by Grimmond and Oke, Macdonald et al., and Theurer, (hereinafter referred to as HB, Thumb, MGH, and Theurer, respectively) are examined first, and a new model is proposed and validated.

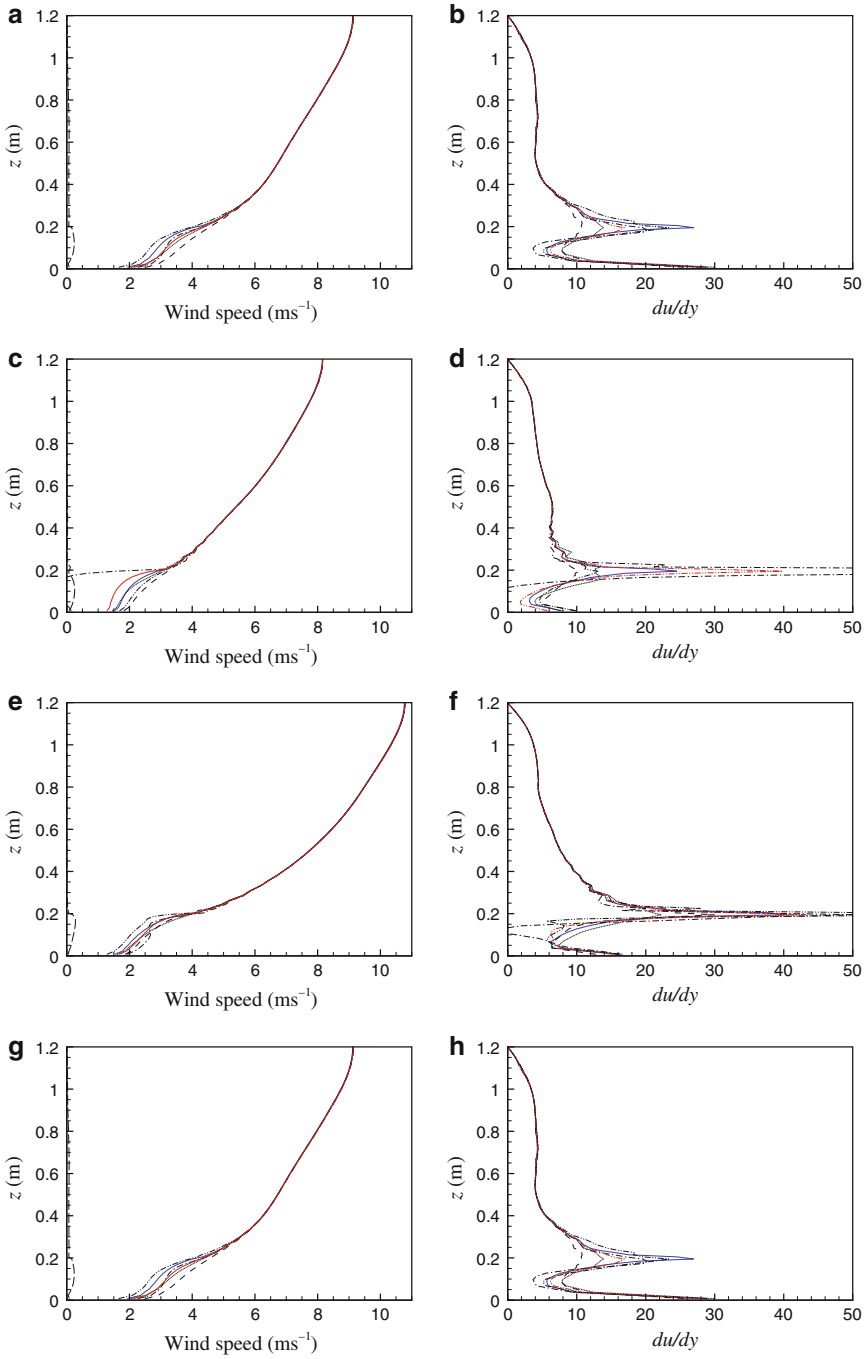

Fig. 8 Velocity profiles and velocity gradient are compared for time-space average and four-point average. **a**, **b** Array A with wind direction 0°; **c**, **d** array A with wind direction 40°; **e**, **f** array B with wind direction 30°; **g**, **h** array B with wind direction 60°; *Blue solid line*: $\langle \overline{u} \rangle$ by LES; *dashed, dashed-dot, dotted and dashed-dot-dot lines*: $\overline{u}$ by LES at point 1, 2, 3 and 4, respectively; *red solid line*: four-point average by LES; *long dashed line in wind speed plots*: $|\langle \tilde{u}\tilde{w} \rangle|^{0.5}$ by LES

4.1 Existing Models for Estimating Surface Roughness Parameters

From real scale observations and wind-tunnel experiments, Theurer (1993) proposed a morphological model,

$$\frac{d}{H} = 1.67\lambda_p, \tag{6}$$

for $\lambda_p < 0.6$,

$$\frac{z_0}{H} = 1.6\lambda_f(1 - 1.67\lambda_p), \tag{7}$$

for $\lambda_f < 0.25$, which depends on λ_p as well as λ_f. Later, Macdonald et al. (1998) extended Lettau (1969)'s model to a general form without any approximations,

$$\frac{z_0}{H} = \left(1 - \frac{d}{H}\right)\exp\left(-\left(0.5\beta\frac{C_D}{\kappa^2}\left(1 - \frac{d}{H}\right)\lambda_f\right)^{-0.5}\right), \tag{8}$$

where the drag coefficient $C_D = 1.2$, and $\beta = 0.55$ for a square array and $\beta = 1$ for a staggered array. The zero-plane displacement length is given by an empirical relation

$$\frac{d}{H} = 1 + A^{-\lambda_p}(\lambda_p - 1), \tag{9}$$

where the empirical constant A is 4.43 and 3.59 for staggered and square arrays, respectively. Unlike Theurer's model, this model does not depend on λ_f.

Grimmond and Oke (1999) suggested a rule-of-thumb model in which z_0 and d linearly increase with H,

$$\frac{z_0}{H} = 0.1, \tag{10}$$

$$\frac{d}{H} = 0.7. \tag{11}$$

Despite its simplicity, as will be shown later, this model performs relatively well compared with other complicated models.

Recently, Hanna and Britter (2002) presented a morphological model

$$\frac{z_0}{H} = \lambda_f \tag{12}$$

for $\lambda_f < 0.15$,

$$\frac{z_0}{H} = 0.15 \tag{13}$$

for $\lambda_f \geq 0.15$,

$$\frac{d}{H} = 3\lambda_f \tag{14}$$

for $\lambda_f < 0.05$,

$$\frac{d}{H} = 0.15 + 5.5(\lambda_f - 0.05) \tag{15}$$

for $0.05 < \lambda_f < 0.15$,

$$\frac{d}{H} = 0.7 + 0.35(\lambda_f - 0.15) \tag{16}$$

for $0.15 < \lambda_f < 1.0$ (if $\lambda_f > 1.0$ then set $\lambda_f = 1.0$). This model depends on λ_f only. Jackson (1981) showed that the zero-plane displacement corresponds to the height at which the mean drag appears to act on the flow. He recommended $d/H = 0.7$ for common types of roughness elements.

4.2 Proposition of a New Model

The morphological models discussed in the previous section were applied to the uniform arrays used in the wind-tunnel experiments. Roughness parameters predicted by these models are compared with the parameters determined using the best-fit method in Fig. 9. Most models significantly overestimate z_0 as compared with not only the best-fit data but also the experimental data of Inagaki and Kanda (2008) and Cheng and Castro (2002b). On the other hand, HB and the Thumb model predict d relatively accurately. For the array C, z_0/H does not vary significantly, ranging between 0.01 and 0.02, while λ_f increases from 0.12 to 0.38 by a factor of 3. d/H of array C approaches unity when λ_f exceeds 0.3 or when θ is large. The behaviour of d indicates that the flow regime of array C at this high λ_f belongs to the skimming flow, which is not frequently observed in urban areas (Hanna and Britter 2002). Hence the dataset of array C was not used in the derivation of a new model. Using datasets of arrays A and B, a new morphological model, especially suitable for the obstacle arrays modelling tall and slender buildings, is proposed here.

Taking a linear best-fit with the constraint that $z_0 = 0$ at $\lambda_f = 0$, a relation for z_0 is suggested as follows

$$\frac{z_0}{H} = 0.164\lambda_f. \tag{17}$$

Although a constraint for λ_f is not specified here, the valid range of λ_f is $0 < \lambda_f < 0.5$, which is the range of the present wind-tunnel experiments.

Using a similar approach with a constraint that $d = 0$ at $\lambda_f = 0$ yields the model equation for d,

$$\frac{d}{H} = 5.5\lambda_f \tag{18}$$

for $0 < \lambda_f < 0.14$,

$$\frac{d}{H} = 0.77 \tag{19}$$

for $\lambda_f > 0.14$. Here the constant 0.77 was calibrated so that the model equation is continuous at $\lambda_f = 0.14$. Figure 9 shows that d predicted by the present model is similar to predictions of other models such as HB and Thumb models that are based on λ_f or on H. However, predictions by the Thumb model depart from the experimental data for $\lambda_f < 0.12$. Morphological models depending on λ_p such as Theurer and MGH significantly underestimate d, clearly indicating that the frontal area is a more crucial parameter than the plan area. Recent measurements of z_0 and d over uniformly distributed cube arrays in the outdoor experiments by Inagaki and Kanda (2008), wind-tunnel experiments by Cheng and Castro (2002b), and direct numerical simulation by Coceal et al. (2006) all support our relation, although their cases correspond to one case of $\lambda_f = 0.25$ (Fig. 9). Experimental estimation of z_0 by Iyengar and

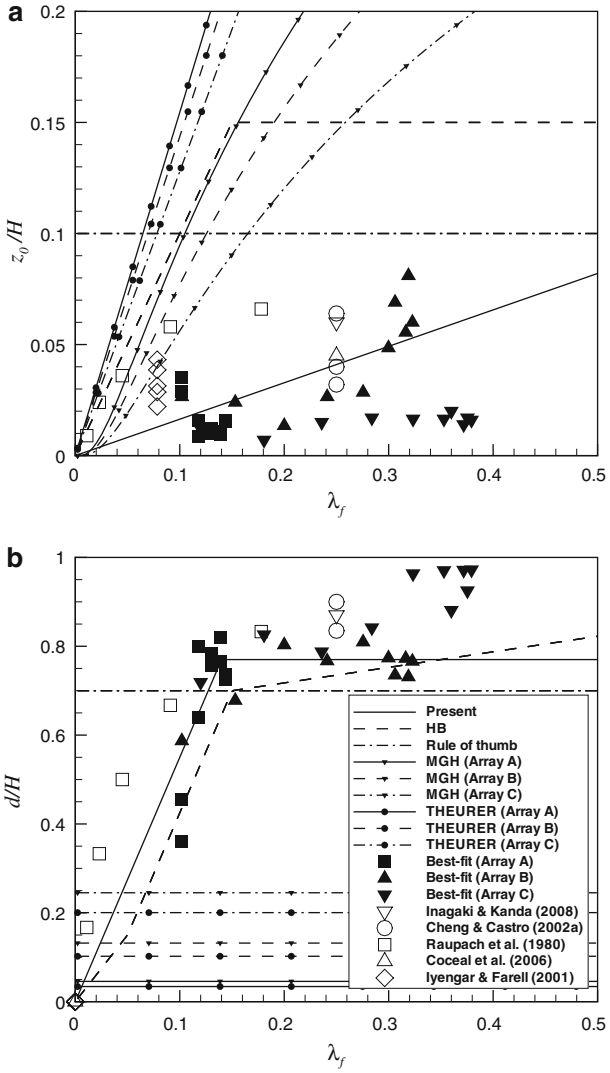

Fig. 9 Distributions of z_0/H and d/H as a function of λ_f. Predictions by MGH and Theurer models are drawn for three λ_p cases

Farell (2001) is rather close to our model although the corresponding λ_f is small. Raupach et al. (1980)'s wind-tunnel measurement yields z_0 larger than our model's estimation, but z_0/H remains less than 0.07 even for a large λ_f.

Roughness parameters, u_*, z_0, and d, estimated by the five morphological models including the present model and the best-fit method for arrays A, B, and C are shown in Figs. 10, 11, and 12, respectively. Here, u_* was calculated by matching the measured wind speed at the height $z = 5H$ using the estimated z_0 and d by Eq. 1. For all wind directions, the present morphological model shows better agreement with the best-fit method than other models in the estimation of u_*. Although data for array C were not used in the derivation of the present model, the estimation of u_* by our model is closest to the best-fit approximation.

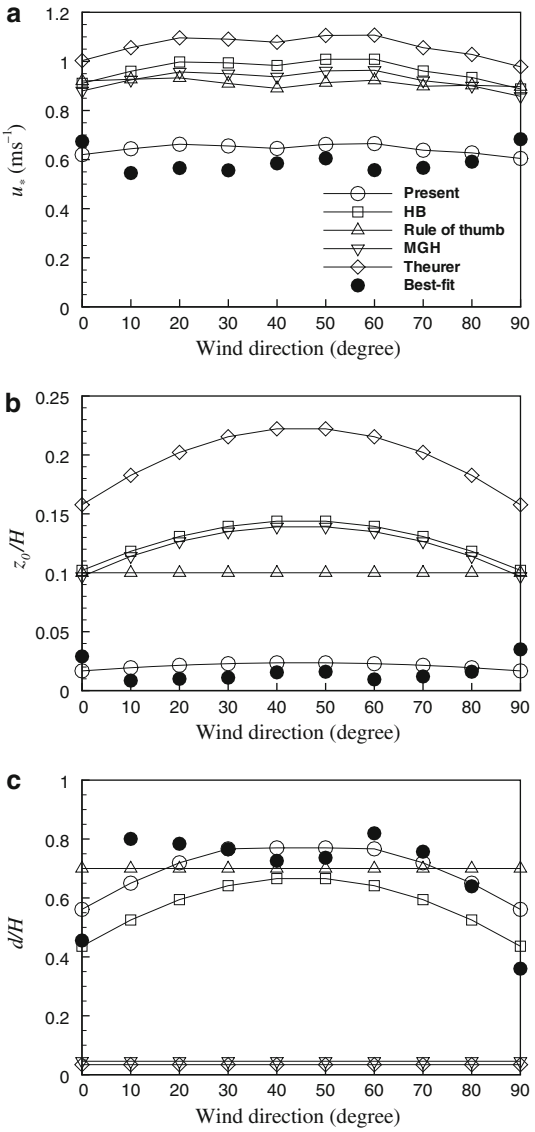

Fig. 10 Distributions of **a** the friction velocity; **b** roughness length; and **c** zero-plane displacement as a function of the wind direction in the array A. For the estimation of u_* using the different morphological models see text

Another method to assess a model is to investigate whether a mean wind-speed profile correctly represents a logarithmic profile. Nondimensional velocity profiles obtained using roughness parameters, which were estimated by morphological models and the best-fit method, are compared in Fig. 13. Clearly, the velocity profiles drawn from the best-fit method approximate well the standard log profile except for small values of $(z - d)/z_0$, i.e., in the vicinity of the rooftops of roughness elements. Log regions attained by the HB, Theurer, and Thumb models quickly deviate from the log profile when the value of $(z - d)/z_0$ decreases. Overall, their log ranges are shorter than those predicted by the best-fit method and the present model although the width of log range does not guarantee good performance of the model tested. MGH and the present model predict profiles best matched to the log profile. It is

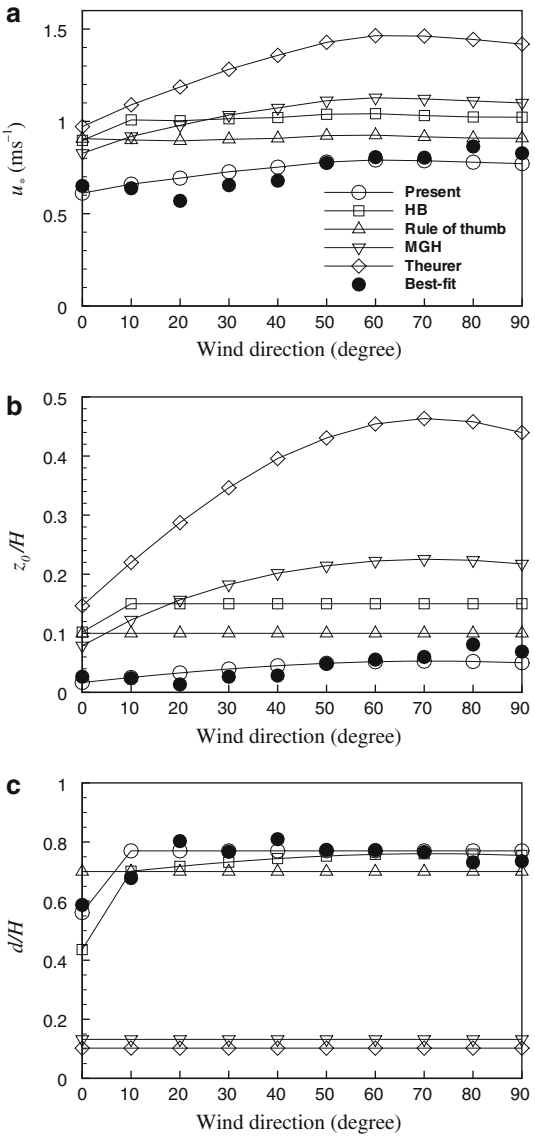

Fig. 11 Distributions of **a** the friction velocity; **b** roughness length; and **c** zero-plane displacement as a function of the wind direction in the array B. For the estimation of u_* using the different morphological models see text

interesting to recognize that the MGH model produces good log-law profiles while z_0 and u_* are overestimated and d is underestimated. The overestimation of the friction velocity yields over-predicted turbulence, leading to falsely enhanced dispersion.

Pollutant dispersion is influenced not only by the mean wind speed but also by turbulent fluctuations. In an urban boundary layer, the turbulence intensity is enhanced by the mechanical shear due to immersed bluff bodies. Due to the local similarity assumption, turbulence levels in the urban boundary layer can be approximated by the following constant stress distribution (Britter and Hanna 2003)

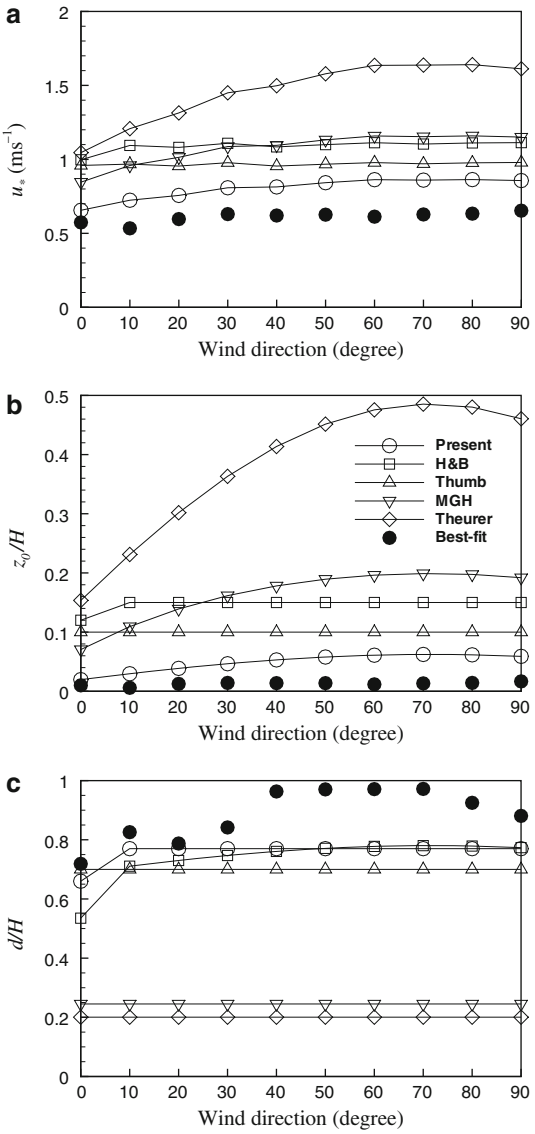

Fig. 12 Distributions of **a** the friction velocity; **b** roughness length; and **c** zero-plane displacement as a function of the wind direction in the array C. For the estimation of u_* using the different morphological models see text

$$\sigma_u = au_*, \tag{20a}$$

$$\sigma_v = bu_*, \tag{20b}$$

$$\sigma_w = cu_*, \tag{20c}$$

where the a, b, and c are nondimensional model coefficients. Roth (2000) suggested $a = 2.4 \pm 0.25$, $b = 1.91 \pm 0.26$, and $c = 1.27 \pm 0.26$ from comprehensive observations of turbulence over numerous cities. Hanna and Britter (2002) recommended values $a = 2.4$, $b = 1.9$, and $c = 1.3$ analogous to those of Roth (2000). Recently, Inagaki and Kanda (2008) showed that the coefficients have similar values that are obtained from field experiments. They showed that turbulence intensity decreases with the height in the vicinity of rooftops.

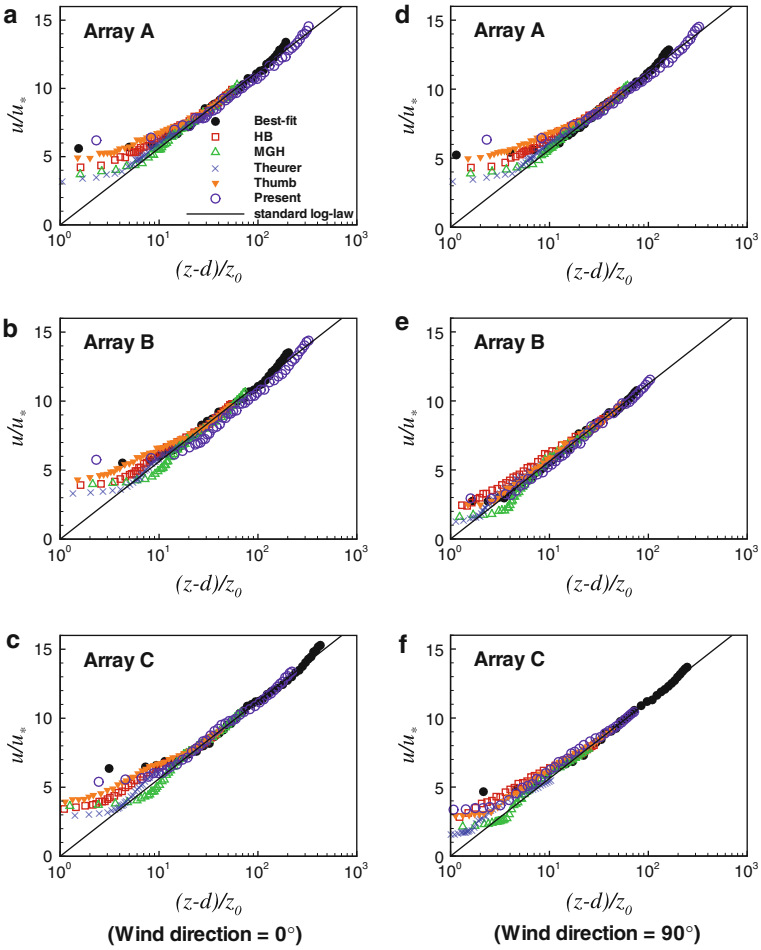

Fig. 13 Profiles of the measured mean wind speed normalized by roughness parameters that are estimated using morphological models as shown in legends for wind directions: **a**–**c** 0 and **d**–**f** 90 degrees

Similar behaviour is observed in the present experiments (Fig. 14). Vertical lines in Fig. 14 indicate the turbulence levels predicted by Eq. 20 with values for a, b, and c recommended by Hanna et al. (2002). The friction velocity used here was obtained using the best-fit method. In most cases, models overestimate turbulence intensity. It should be mentioned that turbulence levels predicted by other morphological models are much higher than the levels shown in Fig. 14, since u_* estimated by those models are larger than that estimated by the best-fit method due to underestimation of z_0. A conjecture for overrestimation of a, b, and c is that our roughness elements are tall and sparsely distributed while most previous studies were for cubical elements. Slender bodies might not disturb the incoming flow as much as cubes do.

4.3 Application to a Scale Model of an Urban Area

In this section, the proposed model and other models are applied to a non-uniform roughness case, a scale model of a real urban area, for further assessment. Measurement locations in the non-uniform urban model for four wind directions are provided in Fig. 5. Morphological

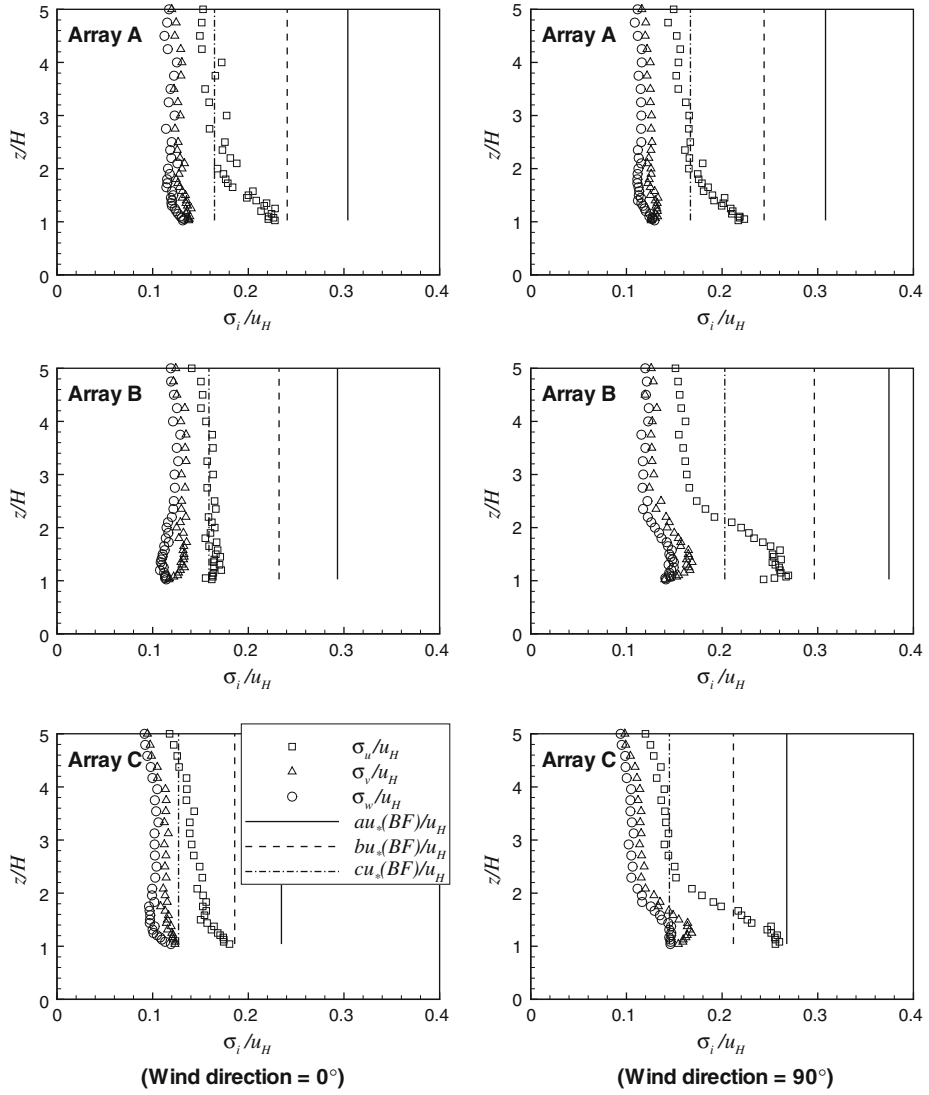

Fig. 14 Non-dimensional turbulence levels deduced from experiments (*symbols*) and the present model (*lines*). In legends, $u_*(BF)$ represents the friction velocity obtained by the best-fit method

parameters, λ_f and λ_p, are computed using rasterized building height data, in the form of digital elevation map (DEM), which was converted from the vector formatted CAD data. In this way the algorithms to compute the λ parameters and to divide lot areas are easily carried out. As was denoted by Martilli (2009), the best simplified morphology should have the same values of λ parameters as the real morphology (or as the miniature in this study). In the DEM, buildings are composed of grid cells, which are sufficiently fine for a good representation of the building geometry. The sensitivity of λ parameters to the grid resolution was tested to confirm that λ_f and λ_p are obtained precisely. The test showed that λ_p approached an asymptotic value when the number of grids was greater than 300×300 (one grid cell corresponds

Table 2 Mean building height (H), standard deviation of the building height ($sd(H)$), and the number of buildings located in each zone (N)

Wind direction	Zone number	1	2	3	4	5	6	7	8	9	10
	H	78	89	123	98	85	98	96	79	123	67
180°	$sd(H)$	34	33	36	43	40	44	47	45	50	19
	N	42	62	45	35	53	64	15	28	32	8
Wind direction	Zone number	11	12	13	14	15	16	17	18	19	20
	H	84	75	87	101	89	90	115	96	82	110
225°	$sd(H)$	35	29	42	42	34	51	48	37	53	39
	N	42	64	56	40	60	48	19	30	23	60
Wind direction	Zone number	21	22	23	24	25	26	27	28	29	30
	H	72	89	107	89	80	103	110	87	103	96
270°	$sd(H)$	30	39	52	38	28	52	63	33	42	34
	N	63	53	53	57	55	38	38	36	18	54
Wind direction	Zone number	31	32	33	34	35	36	37	38	39	40
	H	102	85	96	87	74	95	89	68	104	122
315°	$sd(H)$	47	39	47	33	26	41	39	35	48	23
	N	50	58	41	63	57	36	60	48	28	29

See Fig. 5 for the definition of the wind direction. The length unit is mm

to 6 m × 6 m in the real city). On the other hand, λ_f converges rather slowly, thus it achieves an asymptotic value at the resolution of 600 × 600 (3 m × 3 m in the real city). Distribution of λ parameters are found to be quite inhomogeneous in space. It is also found that λ_f is sensitive to the wind direction in a real urban area, in which the majority of buildings with a large width-to-depth ratio face the south. In this study, all morphological parameters for the non-uniform array were obtained with the resolution of 2400 × 2400 (0.75 m × 0.75 m resolution in the real city).

The mean building height, H, of a lot area is computed by weighting the plan area of buildings,

$$H = \frac{\sum_{i=1}^{N} a_p^i h^i}{\sum_{i=1}^{N} a_p^i}, \tag{21}$$

where N, a_p^i, and h^i denote the number of buildings in a lot area, sectional area and height of a building, respectively. The specification of an area around each measurement point depicted by a number as shown in Fig. 5 was made such that a sufficient number of obstacles are included in the windward area of the point. The computed mean height, standard deviation of building height, and the number of buildings per each lot area are listed in Table 2.

It has been known that an equilibrium boundary layer develops after a number of rows of obstacles in a uniform array. In general, there are no rows of obstacles in real cites, nonetheless we can apply guidelines for sufficient fetch from previous studies. For example, Hanna and Britter (2002) recommended five to ten or more rows, equivalently $MAX(20\,\text{m}, 10H)$ in length, for the establishment of an equilibrium boundary layer. Cheng and Castro (2002a) showed that $160z_0$ is required to achieve an equilibrium boundary layer in the 2-D rod array.

If the rule-of-thumb is used as a basis, $16H$ is an equivalent fetch to the criterion. Considering this and the mean building height of the Daejeon city scale model, $H \simeq 0.1$ m, fetches of 1.5, 0.5, and 0.5 m are selected for the windward, leeward, and both spanwise directions from a measurement location selected as shown in Fig. 5. Thus all rectangular lot areas have A_T of 2 m $\times$ 1 m as shown in Fig. 5. For this purpose, Kastner-Klein and Rotach (2004) used an upwind elliptical area.

For the extraction of z_0, d, and u_*, a conventional method was applied. A morphological model provides z_0 and d for given λ_f and λ_p. Then u_* is estimated by Eq. 1 using the mean wind speed measured at the reference height, $z = 0.4$ m. Then, we evaluate the model performance by comparing u_* and a friction velocity estimated by taking the maximum from the vertical profile of $(-\overline{u'w'})^{0.5}$ regardless of height. The best-fit method is not used here since the spatially-averaged mean speed cannot be properly calculated from experimental data due to the building geometry and inhomogeneity of building arrangement. z_0, d, and u_* for each lot area are illustrated in Figs. 15 and 16. The Theurer model performs relatively well when $\lambda_f \simeq \lambda_p$. For example, for lot areas 1, 4, 7, and 8, and all lot areas for the wind direction 270°, u_* predicted by the Theurer model does not show significant excursion from the measured data. Figure 15b also shows that d predicted by λ_p-based models (i.e., Theurer and MGH) is smaller than that predicted by λ_f-based models. Opposite behaviour is observed in the estimation of z_0, which is a well-known problem of partitioning between z_0 and d. Thus in an urban area that is composed of tall buildings (i.e., $\lambda_f/\lambda_p > 1$), λ_p-based models likely fail to produce representative z_0 and d.

Figure 16 shows that the least scattering is observed with the Thumb model, but it tends to overestimate the friction velocity in the majority of cases. HB, MGH, and Theurer overestimate the friction velocity also, with greater scattering. Figure 16 clearly shows that the friction velocity is best predicted by the present model in most lot areas. It is interesting to note that there is a good correlation between z_0 and u_* (see Fig. 15a, c). It can be conjectured that u_* is determined by z_0 in a more sensitive manner than by d. From Eq. 1, the sensitivities of u_* with respect to z_0 and d can be obtained by

$$\frac{\partial u_*}{\partial z_0}\frac{z_0}{u_*} = \frac{1}{\ln(z-d)/z_0}, \tag{22}$$

$$\frac{\partial u_*}{\partial d}\frac{d}{u_*} = \frac{1}{\ln(z-d)/z_0}\frac{d}{z-d}. \tag{23}$$

The ratio of these sensitivities becomes

$$\frac{(z_0/u_*)\partial u_*/\partial z_0}{(d/u_*)\partial u_*/\partial d} = \frac{z}{d} - 1, \tag{24}$$

which is much larger than 1 since the reference height is much higher than d, confirming the conjecture. Therefore, we carefully conclude that an overestimation of z_0 directly leads to an overestimation of u_*. This trend was also observed in the uniform arrays (see Figs. 10, 11, and 12).

4.4 Effect of the Height Variation

For a more quantitative assessment of the proposed model, we investigate the effect of the height variation in the non-uniform array through the velocity difference between experimental data and a logarithmic profile within $H < z < z_b$ at a measurement location where an error is defined by

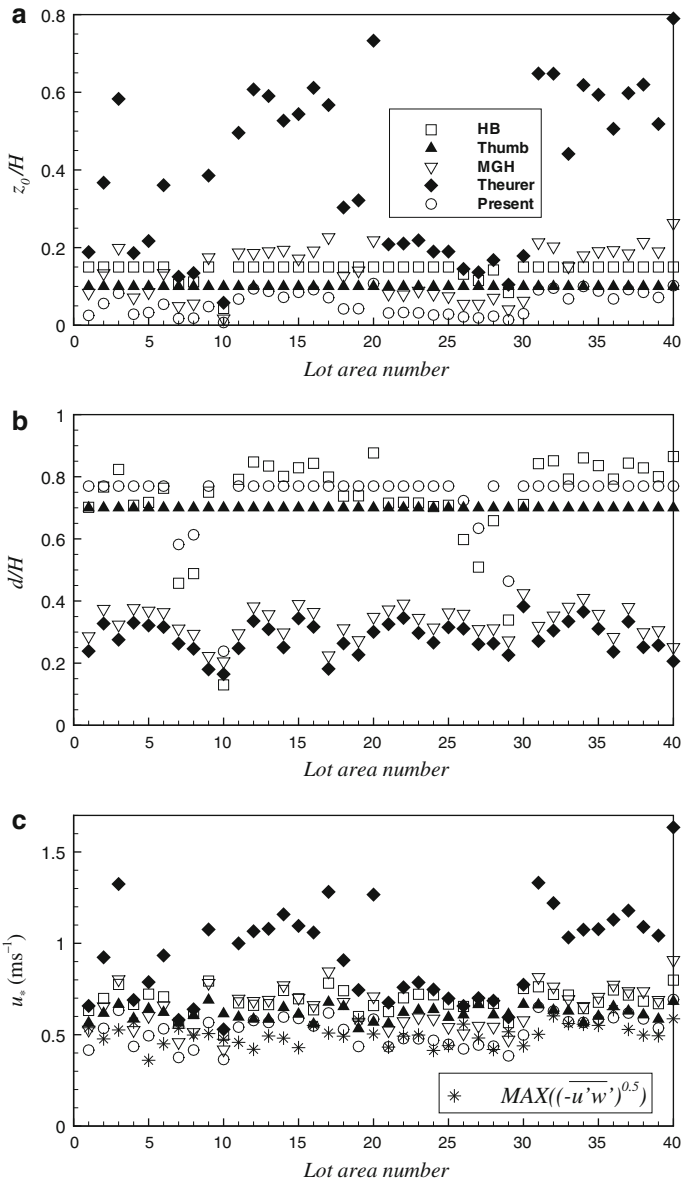

Fig. 15 **a** Roughness length, **b** zero-plane displacement, and **c** friction velocity of each zone in the nonuniform roughness array

$$\varepsilon = \frac{\int_H^{z_b} (u_e - u_l)^2 \, dz}{\int_H^{z_b} u_e^2 dz}, \tag{25}$$

where z_b is 1 m for the uniform arrays and 0.4 m for the non-uniform array, u_e and u_l represent experimental and logarithmic wind speeds, respectively, and are constructed using the roughness parameters estimated by the proposed model. Again, the assumption that the log

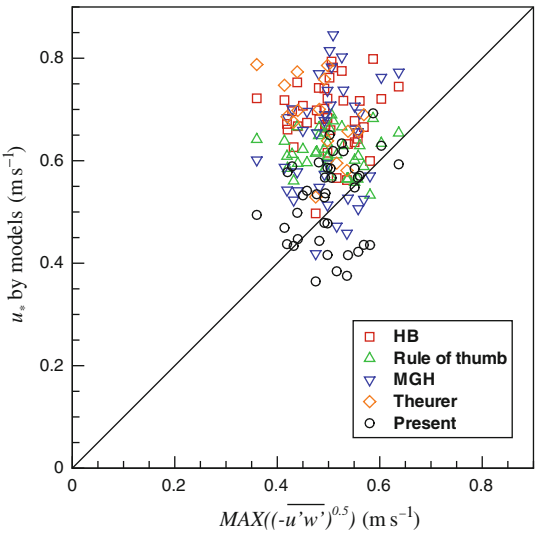

Fig. 16 Friction velocities measured in the experiments and predicted by different models

profile is valid in the region right above H was based on our observation for uniform arrays. The error computed at all measurement locations in the non-uniform array is presented in terms of the standard deviation of the building height along with the upper and lower bounds of the error obtained in the uniform arrays that have zero standard deviation of the height in Fig. 17a. Velocity profiles at locations 12 and 33 where the minimum and maximum errors are found, respectively, are also shown in Fig. 17b and c. Figure 17a shows that the scattered errors are very weakly correlated with the standard deviation of the building height in the scale model of the urban area, and the correlation coefficient is 0.24. It is noteworthy that the error in a non-uniform array is often found within the range of the error observed in the uniform arrays. Thus it can be suggested that the height variability is not a crucial factor that deteriorates performance of the morphological model when applied to a real urban area.

In addition to the height variation, another factor is found to seriously influence the error. The error is found to be small when the number of buildings is evenly distributed in the upstream region of a measurement location (Fig. 17b). This trend is in some sense obvious since the morphological models were derived for uniform arrays. It should be noted that since the velocity profiles measured in the inhomogeneous array do not represent the spatially-averaged velocity, local disturbances by a building adjacent to a measurement location could severely affect the measured velocity. For example, the measured velocity at location 33 (Fig. 17c) is disturbed by the building at 0.5 m ahead of the location. The maximum error is found at this location although the height variability is not largest.

5 Conclusions

We have carried out wind-tunnel experiments over two kinds of roughness arrays to assess urban morphological models: uniformly distributed rectangular slender prisms and a scale model of a real urban area. From the best-fit approximation of wind-speed profiles measured for the uniform roughness arrays, the roughness length, zero-plane displacement, and friction velocity were extracted. A comparison of predictions by preexisting morphological models

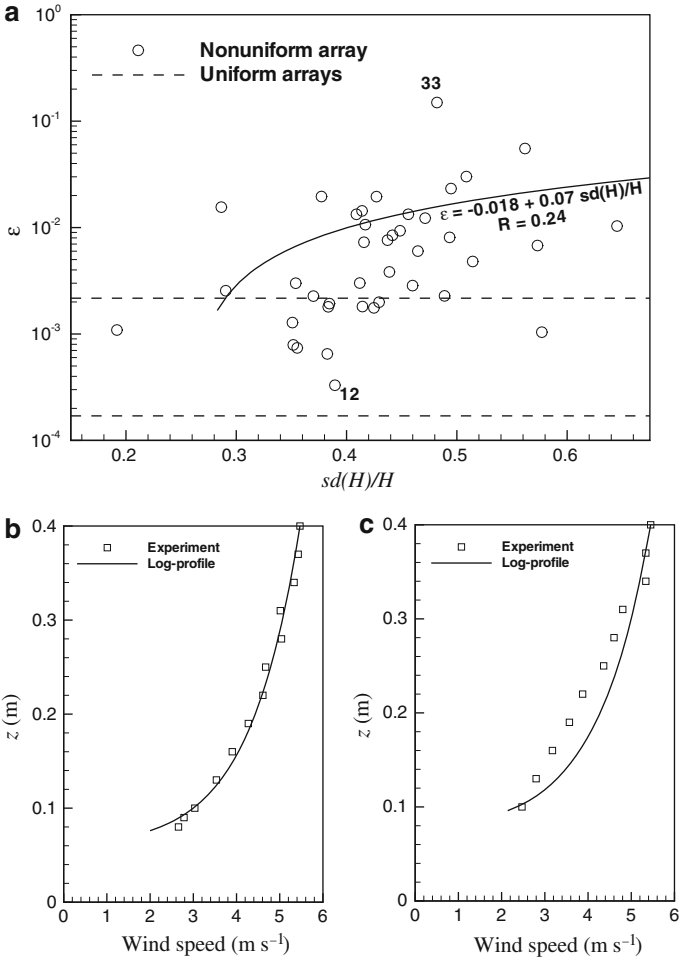

Fig. 17 **a** Error defined by the velocity difference between an experimental value and a logarithmic profile at a measurement location in the non-uniform array (*symbol*). Two measurement locations are indicated by *numbers*. *Dashed lines* are the upper and lower bounds of the error for the uniform arrays. *Solid line* is the linear fit of scattered errors with the correlation coefficient, $R = 0.24$; **b**, **c** experimental and logarithmic velocity profiles at locations 12 and 33, respectively

against theses roughness parameters estimated by a best-fit method clearly shows that most models overestimate z_0, leading to overprediction of u_*. The overestimation may due to that the models are based on the roughness array with high packing density or stocky obstacles such as a cube array and urban area covered with low story buildings. As shown in Grimmond and Oke (1999) the roughness parameters widely scattered according to urban morphologies. The data provided in the present study can be placed in the lower part of envelopes suggested by them. A new morphological model is proposed and validated through a comparison of the estimated u_*^2 and measured Reynolds shear stress. A further assessment of morphological models including the newly proposed model was made in a scale model experiment. The proposed model showed a superior predictive capability to other previous models.

It was also found that the error defined by the velocity difference between experimental data and the estimated log profile is weakly correlated with the building height variation in a lot area. A more significant factor influencing the error appears to be the spatial inhomogeneity of the building distribution.

Finally it is worthwhile to mention that morphological models that do not rely on λ_p, showed better agreement with experimental data. The reason can be inferred, since for the type of urban area in which buildings have the high ratio of width to depth, λ_f is the more important parameter than λ_p since λ_f better represents the effect of the wind direction. It was shown that inhomogeneity of λ_f was significant in the urban area considered in this study.

Acknowledgments This research was supported by the Agency for Defense Development (ADD) and the National Research Foundation of Korea through Grants 20090093134 and R31-2008-000-10049-0 (WCU Program).

References

Bentham T, Britter R (2003) Spatially averaged flow within obstacle arrays. Atmos Environ 37(15): 2037–2043

Britter R, Hanna S (2003) Flow and dispersion in urban areas. Annu Rev Fluid Mech 35(1):469–496

Cheng H, Castro I (2002a) Near wall flow development after a step change in surface roughness. Boundary-Layer Meteorol 105(3):411–432

Cheng H, Castro I (2002b) Near wall flow over urban-like roughness. Boundary-Layer Meteorol 104(2): 229–259

Christen A, Rotach M, Vogt R (2009) The budget of turbulent kinetic energy in the urban roughness sublayer. Boundary-Layer Meteorol 131(2):193–222

Cionco RM (1965) A mathematical model for air flow in a vegetative canopy. J Appl Meteorol 4(4):517–522

Coceal O, Thomas T, Castro I, Belcher S (2006) Mean flow and turbulence statistics over groups of urban-like cubical obstacles. Boundary-Layer Meteorol 121(3):491–519

Coceal O, Thomas T, Belcher S (2007) Spatial variability of flow statistics within regular building arrays. Boundary-Layer Meteorol 125(3):537–552

Counihan J (1971) Wind tunnel determination of the roughness length as a function of the fetch and the roughness density of three-dimensional roughness elements. Atmos Environ (1967) 5(8):637–642

Grimmond C, Oke T (1999) Aerodynamic properties of urban areas derived from analysis of surface form. J Appl Meteorol 38(9):1262–1292

Hagishima A, Tanimoto J, Nagayama K, Meno S (2009) Aerodynamic parameters of regular arrays of rectangular blocks with various geometries. Boundary-Layer Meteorol 132(2):315–337

Hanna S, Britter R (2002) Wind flow and vapor cloud dispersion at industrial and urban sites. CCPS, New York, 208 pp

Hanna S, Tehranian S, Carissimo B, Macdonald R, Lohner R (2002) Comparisons of model simulations with observations of mean flow and turbulence within simple obstacle arrays. Atmos Environ 36(32): 5067–5079

Hanna S, Brown M, Camelli F, Chan S, Coirier W, Hansen O, Huber A, Kim S, Reynolds R (2006) Detailed simulations of atmospheric flow and dispersion in downtown Manhattan. Bull Am Meteorol Soc 87: 1713–1726

Inagaki A, Kanda M (2008) Turbulent flow similarity over an array of cubes in near-neutrally stratified atmospheric flow. J Fluid Mech 615:101–120

Iyengar AKS, Farell C (2001) Experimental issues in atmospheric boundary layer simulations: roughness length and integral length scale determination. J Wind Eng Ind Aerodyn 89:1059–1080

Jackson PS (1981) On the displacement height in the logarithmic velocity profile. J Fluid Mech 111:15–25

Jiménez J (2004) Turbulent flows over rough walls. Annu Rev Fluid Mech 36(1):173–196

Kastner-Klein P, Rotach M (2004) Mean flow and turbulence characteristics in an urban roughness sublayer. Boundary-Layer Meteorol 111(1):55–84

Lettau H (1969) Note on aerodynamic roughness parameter estimation on the basis of roughness element description. J Appl Meteorol 8:828–832

Macdonald R (2000) Modelling the mean velocity profile in the urban canopy layer. Boundary-Layer Meteorol 97(1):25–45

Macdonald R, Griffiths R, Hall D (1998) An improved method for the estimation of surface roughness of obstacle arrays. Atmos Environ 32(11):1857–1864
Macdonald R, Carter S, Slawson P (2000) Measurements of mean velocity and turbulence statistics in simple obstacle array at 1:200 scale. Thermal Fluids Report 2000–1, University of Waterloo, Canada, 130 pp
Macdonald RW, Carter Schofield S, Slawson PR (2002) Physical modelling of urban roughness using arrays of regular roughness elements. Water Air Soil Pollut Focus 2(5):541–554
Martilli A (2009) On the derivation of input parameters for urban canopy models from urban morphological datasets. Boundary-Layer Meteorol 130(2):301–306
McDermott R, McGrattan K, Hostikka S, Floyd J (2009) Fire dynamics simulator (version 5) technical reference guide volume 2: verification. National Institute of Standards and Technology, 75 pp
McGrattan K, Hostikka S, Floyd J, Baum H, Rehm R, Mell W, McDermott R (2009a) Fire dynamics simulator (version 5) technical reference guide volume 1: mathematical model. National Institute of Standards and Technology, 108 pp
McGrattan K, Hostikka S, Floyd J, McDermott R (2009b) Fire dynamics simulator (version 5) technical reference guide volume 3: validation. National Institute of Standards and Technology, 298 pp
Petersen R (1997) A wind tunnel evaluation of methods for estimating surface roughness length at industrial facilities. Atmos Environ 31(1):45–57
Ploss A, Castro I, Cheng H (2000) The surface region of rough wall boundary layers. In: Dopazo C (ed) Advances in turbulence VIII. International Center for Numerical Methods in Engineering, pp 455–459
Raupach MR, Thom AS, Edwards I (1980) A wind-tunnel study of turbulent flow close to regularly arrayed rough surfaces. Boundary-Layer Meteorol 18(4):373–397
Raupach MR, Coppin PA, Legg BJ (1986) Experiments on scalar dispersion within a model plant canopy, Part I: the turbulence structure. Boundary-Layer Meteorol 35(1):21–52
Rotach M (2001) Simulation of urban-scale dispersion using a Lagrangian stochastic dispersion model. Boundary-Layer Meteorol 99(3):379–410
Roth M (2000) Review of atmospheric turbulence over cities. Q J Roy Meteorol Soc 126(564):941–990
Santiago JL, Martilli A (2010) A dynamic urban canopy parameterization for mesoscale models based on computational fluid dynamics Reynolds-averaged Navier-Stokes microscale simulations. Boundary-Layer Meteorol 137(3):417–439
Schlichting H, Gersten K (2000) Boundary-layer theory, 8th edn. Springer, Germany, 799 pp
Shah KB (1998) Large eddy simulations of flow past a cubic obstacle. PhD thesis, Stanford University, 212 pp
Snyder WH, Castro IP (2002) The critical Reynolds number for rough-wall boundary layers. J Wind Eng Ind Aerodyn 90(1):41–54
Stull R (1988) An introduction to boundary layer meteorology. Kluwer Academic Publisher, The Netherlands, 666 pp
Tamura T (2008) Towards practical use of LES in wind engineering. J Wind Eng Ind Aerodyn 96(10–11):1451–1471
Theurer W (1993) Dispersion of ground-level emissions in complex built-up areas. PhD thesis, Doctoral thesis, Department of Architecture, University of Karlsruhe, Germany
Theurer W, Baechlin W, Plate EJ (1992) Model study of the development of boundary layers above urban areas. J Wind Eng Ind Aerodyn 41(1–3):437–448
Visual Numerics Inc. (1997) IMSL STAT/LIBRARY: Fortran subroutines for statistical applications. Visual Numerics Inc., Texas
Werner H, Wengle H (1992) Large-eddy simulation of turbulent flow over and around a cube in a plate channel. In: Turbulent shear flows: selected papers from the eighth international symposium on turbulent shear flows, vol 8. Springer-Verlag, Berlin, pp 155–168